# Olfactory modulation of barrel cortex activity during active whisking and passive whisker stimulation

**Anthony Renard**
Institut Pasteur
**Evan Harrell**
Institut Pasteur
**Brice Bathallier** ( brice.bathellier@cnrs.fr )
Institut Pasteur

**Article**

**Keywords:** Olfaction and touch, 2-photon Calcium Imaging, Central Cross-talk, Facial Nerve Sectioning, Independent Coding

**Posted Date:** March 13th, 2021

**DOI:** https://doi.org/10.21203/rs.3.rs-289925/v1

# Abstract

Rodents depend on olfaction and touch to meet many of their fundamental needs. The joint significance of these sensory systems is underscored by an intricate coupling between sniffing and whisking. However, the impact of simultaneous olfactory and tactile inputs on sensory representations in the cortex remains elusive. To study these interactions, we recorded large populations of barrel cortex neurons using 2-photon calcium imaging in head-fixed mice during olfactory and tactile stimulation. We find that odors alter barrel cortex activity in at least two ways, first by enhancing whisking, and second by central cross-talk that persists after whisking is abolished by facial nerve sectioning. Odors can either enhance or suppress barrel cortex neuronal responses, and while odor identity can be decoded from population activity, it does not interfere with the tactile representation. Thus, barrel cortex represents olfactory information which, in the absence of learned associations, is coded independently of tactile information.


# Introduction

Perception occurs through the coordinated evaluation of information from multiple senses[1]. This coordination is evident when considering the well-documented cross-modal illusions in humans[2–4], such as the ventriloquist illusion, in which erroneous sound localization is generated by visual cues. Illusions reveal strong associations across particular cues from different sensory modalities that can be maintained even if the resulting perception breaks with the physical reality. Such associations are generally useful to improve sensory judgements when information from each sense is scarce or ambiguous. In line with this, multisensory interactions are strongest when unisensory ambiguity is highest[2,5]. This inverse-effectiveness phenomenon is interpreted as an optimal integration of available information[5]. Neurons were identified in the associative cortical areas of monkeys[6,7] and rodents[8,9] which sum inputs representing congruent information from distinct modalities. This simple multisensory integration mechanism can explain inverse effectiveness and most perceptual observations, but not all[10]. A causal link between multisensory integration and associative integration has also been established[8].

While neurons in association cortex do exhibit multimodal coding properties, several studies suggest that cross-modal connections already exist in the primary sensory cortical areas both in primates[11] and rodents[12]. These connections are functional. Most recently, it was shown that direct projections from the primary auditory cortex modulate supragranular primary visual cortex neurons in a context-dependent manner[13–15]. Even if the perceptual impact of such low level auditory-visual interactions remains a puzzle, there is convergent evidence that they sharpen and emphasize cortical representations of the visual stimuli that are coincident with startling sounds[14,15], without a particular congruence of visual and auditory cues. This suggests the existence of multi-sensory mechanisms that are complementary to the classical cross-modal integration observed at associative levels. However, so far, it is unclear whether such interactions represent a generic computational process in primary sensory cortical areas or a feature specific to audition and vision in rodents.

To investigate this question, we focused on another pair of sensory modalities. While primates and humans rely primarily on vision and audition for survival, rodents depend to a much larger degree on olfaction and whisker touch. This reliance is underscored by an exquisite coupling between sniffing and whisking rhythms[16] and by observations that rats can easily solve a task that requires the integration of olfactory and tactile cues[17]. Nevertheless, it is unknown how these two crucial modalities interact in the brain. Activity in barrel cortex is modulated by breathing, and this modulation depends on an intact olfactory pathway[18], but there is no evidence that odor-related information arrives to barrel cortex. To examine the impact of odors on touch processing, we performed 2-photon calcium imaging in barrel cortex of awake mice during precisely controlled olfactory and tactile stimulations. We found that both barrel cortex activity and whisking behavior is impacted by odor stimulation. However, neither abolition of whisking by facial nerve sectioning nor pharmacological blockade of local cholinergic signaling could eliminate odor-related activity in barrel cortex. This indicates that it depends on olfactory-related, secondary projections to the somatosensory system which do not include the cholinergic attentional system. In support of this, odor identity could be readily decoded from barrel cortex population activity, but the presence of olfactory information did not impact the quality of tactile representations. Therefore, our study reveals that, in the absence of learned associations, barrel cortex activity contains olfactory information encoded in dimensions of the neural representations that are orthogonal to the tactile representations.

# Results

### Calcium imaging of L2/3 barrel cortex neurons during olfacto-tactile stimulation

The first difficulty in investigating potential cross-talk between olfactory and tactile processing is to precisely control coincident olfactory and tactile stimulations. To achieve this, we coupled a motorized tactile-object-presenting wheel with a custom-made olfactometer to synchronously present oriented tactile gratings (0° or 90°) and odors (amyl acetate or ethyl butyrate diluted at 0.1%; **Fig. 1a**) to the snout of a mouse. The olfactometer was calibrated with a photoionization detector (PID; **Supplementary Fig. 1**). Awake mice were head-fixed with their nose confined in a constant and isolated air stream to prevent the air flow from causing movements of the whiskers. In dark conditions with infrared backlighting, oriented tactile gratings were brought within range of the whiskers using a linear stage. Whisker interactions with the gratings were recorded with a high-speed infrared camera and breathing was monitored with a pressure sensor placed perpendicular to the odor stream (**Fig. 1d**).

We considered two stimulation contexts (**Fig. 1b**): in the first one, the active context, the animal was free to explore a grating that came into reach of its whiskers; in the second one, the passive context, the inferior and superior buccal branches of the facial nerve were sectioned bilaterally, abolishing whisking, and the tactile stimulation consisted of a single back-and-forth sweep of the grating against the whiskers. In both stimulation contexts, the onset of odor presentation to the nose was precisely synchronized with the time when the grating reached its fixed position (active context) or at first possible contact with the whiskers (passive context).

To record large populations of barrel cortex neurons during presentation of odors and tactile gratings, we performed stereotactic injections of AAV1-syn-GCaMP6s at 3-4 locations in barrel cortex centered around the C2 barrel (AP -1.6, ML -3.3, DV 0.5)[19]. After ~4 weeks, location of the GCaMP6s expression locus in barrel cortex was validated using intrinsic imaging (**Fig. 1c**), and mice were placed under a 2-photon microscope for calcium imaging of large populations of supragranular neurons (imaging depth from 100µm to 250µm). A total of 9714 neurons were recorded in the active whisking context from 20 sessions with 12 mice; and 14408 neurons from 19 sessions with 6 mice in the passive context. Among those populations, 1907 (19.6%) and 5162 (35%) neurons from the active and passive contexts, respectively, were responsive to at least one of the nine stimulation conditions (significance level = 5%; Kruskal-Wallis test) and were kept for analysis. One or two populations at different cortical depths were imaged per mouse in the active context and 1-4 locations in the passive context. Calcium traces from four example neurons illustrate responses to the nine unique stimulus conditions , which include uni- and bimodal stimulus conditions as well as a blank (Fig. 1e), and show that odors can evoke responses in barrel cortex cells (neurons 1 and 2), or can modulate responses to tactile grating (neurons 3 and 4).

### Odors modulate responses in L2/3 barrel cortex in freely whisking head-fixed mice

We first analyzed how odors impact barrel cortex activity in an active whisking context when they are presented with or without tactile gratings (**Fig. 2a**). Diverse response types were present in barrel cortex population (**Fig. 2b**). In the presence of gratings, odors could either enhance or suppress tactile responses (**Fig.2b**, first and second examples), and when presented alone odors could evoke excitatory or inhibitory responses (**Fig. 2b**, third and fourth examples). In some neurons, odors had the same impact whether a grating was present or not (**Fig. 2b**, fourth example).

To quantify these effects at the population level, we compared the average population activity elicited by the gratings presented alone or paired with odors (**Fig. 2c**). For simplicity, these analyses were done by pooling trials with different odors together (for odor specific analysis, see **Fig. 6**). We found no difference in population activity levels when odors were paired with gratings computed over the entire stimulation epoch. However, when we looked at single cells and compared the average activity to gratings alone and gratings with odors in the 2 sec time window following stimulus onset, we found that odors modulated the activity of 21.7% of the neurons (**Fig. 2d**), with both enhanced and suppressed response types. The fraction of cells whose activity was affected by odors was clearly above a 5% false positive rate. Comparing the proportion of neurons impacted by odors with the proportion obtained from shuffling the trial labels confirmed that the proportion is well above chance level (**Fig. 2e**). To account for differences in activity levels between cells regardless of their tactile responsiveness, we computed a modulation index (**Fig. 2f**). Consistently, the distribution of indices revealed a significant impact of odors when compared with the distribution obtained from shuffled data (**Fig. 2f**) and an equal proportion of cells were enhanced or inhibited by odors (**Fig. 2f,** inset).

Similarly, odors presented alone did not impact average responses at the population level compared to double blank stimulation (no odor no grating) (**Fig. 2g**) but at the single cell level, odor responses could be detected in 18.34% (**Fig. 2h-j**) of the neurons, again with an equal proportion of enhanced and inhibited cells (**Fig. 2j,** inset). Note that due to the sound of the tactile presentation wheel, which was present in double blank trials, mice increase whisking at the beginning of double blank trials yielding a weak increase in neuronal activity in barrel cortex (e.g. see **Fig. 3**). Together, these results show that in an active tactile context, odors modulate the activity of some barrel cortex neurons both during free whisking and during whisking into tactile gratings.

## Odors impact whisker dynamics

The mechanisms by which odors can potentially impact barrel cortex activity are numerous. One possibility is that odors motivate whisker movements which generate tactile inputs to barrel cortex as reafferent sensory signals. To explore this possibility, we tracked whisker movements using high-speed videography and an automated whisker tracking algorithm[20], which allowed us to robustly detect and trace ~12 individual whiskers within the full pad at each time point. From this tracking, we calculated the average amplitude, set point, and absolute curvature change across time (**Fig. 3a**). During trials without tactile gratings, odors caused a slight but significant increase in average amplitude, setpoint, and absolute curvature change both within sessions (**Fig. 3b-d**) and between sessions (**Fig. 3b-d**). Similarly, in the presence of tactile gratings, odors caused a significant increase in average amplitude and absolute curvature change (**Fig. 3b-d**). In this condition, setpoint did not change significantly in the presence of odors despites a tendency towards an increase. This is likely due to the restriction of the full whisking range by the gratings. This analysis shows that odors lead to significant changes in whisking parameters. As there is an intricate link between whisking behavior and sniffing, we also checked if breathing was impacted by odors. The amplitude (**Fig. 3e**) and frequency (**Fig. 3f**) of breathing, measured in a 2 sec time window starting at odor onset, was significantly reduced in the presence of odors compared to conditions without odors, even though there was large variability across sessions for breathing frequency (**Fig. 3f**, bottom). Together, these data show that mice modify their orofacial motor programs when presented with odors. Because whisking impacts barrel cortex activity [21,22], this implies that at least a part of the odor-related activity in barrel cortex could be due to modulations of whisking.

## Odor-induced responses persist in the absence of peripheral interaction

To examine if the impact of odors on barrel activity depends on mechanisms that go beyond the peripheral modulation of whisking by odors, we performed recordings in a passive stimulation context in which whisking was prevented by bilateral sectioning of the inferior and superior buccal branches of the facial nerve (**Supplementary Fig. 2**). In this case, because the mice were not able to explore the tactile stimuli, the gratings were swept once forward and backward through the whisker pad (**Fig. 4a**). This

experimental approach generated robust tactile responses in S1 while removing any potential for odor-induced whisking that results in reafferent sensory signals in barrel cortex. Similarly to the active context (**Fig. 2b**), odors impacted barrel cortex activity with both enhancement and suppression (**Fig. 4b**). At the population level, odors still had no effect on the trial-averaged total activity, except for a small increase that was significant within sessions (**Fig. 4c, g**), but not robustly observed between sessions (**Fig. 4c, g**). At the level of single cells, again, we observed significant modulation of responses by odors with equal proportions of enhanced and suppressed cells. For each cell, we compared the average activity to the grating sweeps alone versus the sweeps with odors. In the absence of whisking, average ΔF/F's were still significantly modulated by odors in 8.99% of the neurons (**Fig. 4d, e**; significance level = 5%; Mann-Whitney U test), a proportion that is still significantly above chance level (**Fig. 4e**) and with a significant bias towards enhancement (**Fig. 4f**, inlet). Consistently, the distribution of modulation indices showed a significant impact of odors when compared to shuffled data (**Fig. 4f**). Interestingly, the fraction of odor-modulated neurons in the absence of whisking was significantly lower than in freely whisking mice (8,99% against 21.7%, p = 0.012, Mann-Whitney U test), indicating that the peripheral modulation of whisking by odors generates a significant fraction of odor-related activity in barrel cortex but not all of it.

In the same way, odors presented alone in the passive context also modulated barrel cortex activity with balanced enhancement and suppression. The average population response was equivalent for odor alone and double blank trials(**Fig. 4g**) with a small enhancement within sessions (**Fig. 4g**). A proportion of 10.81% neurons were significantly modulated by odors in this passive context (**Fig. 4h, j**; significance threshold = 5%; MannWhitney U test), which was also significantly above chance level (**Fig. 4i**). Modulation indices also showed a significant impact of odors presented alone on the population of recorded cells (**Fig. 4j**). Again, the absence of whisking produced a decrease in the fraction of cells responsive in the odor-alone context, although not significantly due to variability across sessions (10.81% against 18.34%, p = 0.118, Mann-Whitney U test). Together, this observation shows that along with modulation of whisking behavior, there is a second mechanism by which odors impact barrel cortex activity that is still active when whisking is abolished.

### Odor related activity in S1 does not reflect cholinergic inputs activity.

Since whisking is not the sole factor explaining odor-related activity in S1, we examined if it could result from cholinergic inputs to the cortex. Cholinergic inputs to the cortex from the basal forebrain have very specific effects on excitatory and inhibitory neurons[23–26] and are known to play a role in attentional modulation based on the behavioral context[27–30]. To assess whether they play a role in odor-related modulation of barrel cortex activity, we performed dual local injections of a nicotinic and a muscarinic receptor antagonist (1mM injection of atropine and mecamylamine, **Fig. 5a**) in barrel cortex shortly before running our olfactory-tactile stimulation protocol in animals with their facial nerve sectioned. This pharmacological perturbation of cholinergic signaling did not have a significant effect on the number of cells modulated by odors presented with or without tactile stimulation (**Fig. 5b**). We conclude that

cholinergic signaling is not one of the mechanisms for modulating barrel cortex activity in the presence of odors. In summary, our results show that odors still modulate barrel cortex activity independently of whisking and cholinergic signaling.

### Olfactory information in barrel cortex is mainly independent of tactile representations

Finally, we evaluated the type of information carried by odor-related activity in barrel cortex and to what extent this information interacts with tactile representations. For this, we used centroid classifiers with a stratified 20-fold cross-validation, trained on population activity vectors to discriminate various stimulation conditions. We first asked whether the presence of an odor was discernible in the population activity by training a classifier to discriminate bimodal trials from tactile only trials or to discriminate odor only trials against blank trials in mice with facial nerve sectioning (**Fig. 6a, b**; same analysis for the active whisking context shown in **Supplementary Fig. 3**). A proportion of 86.4% of the odor only against blank trials were correctly classified and 71.2% of the bimodal against tactile only trials correctly classified using activity from 1 to 2 seconds after stimulus presentation. This high performance of the classifier in both cases shows that information about the presence or absence of an odor is robustly encoded in barrel cortex. Next, we examined if the olfactory information present in barrel cortex was specific to the type of odor presented. Amyl acetate and ethyl butyrate are two very distinct chemicals which are well discriminated in circuits of the olfactory system[31]. Interestingly, when training classifiers to discriminate amyl acetate and ethyl butyrate trials, classification performance was well above chance level with 68.5% trials correctly classified (**Fig. 6d**). These effects were robust enough to be present across sessions (**Supplementary Fig. 3**) and olfactory information was also present during silencing of cholinergic inputs although less pronounced likely due to the reduced number of sessions (**Supplementary Fig. 4**). Hence, odor-related activity in barrel cortex is sufficiently precise to decode some information about odor identity.

This observation raises the question whether the presence of olfactory information in barrel cortex has any impact on the tactile representations or if the two representations are somewhat independent.

To answer this question we quantified whether classifiers discriminating the two different tactile grating orientations presented to the animal were impacted by odor-driven activity. Tactile grating orientation classification could be easily performed by barrel cortex populations, especially in facial nerve sectioned animals (**Fig. 6c**). To evaluate the impact of coincident odors, we trained a classifier to discriminate population activity for the two grating orientations using a training set of trials without odors. We then measured the performance of the classifier using a test set of trials with odors and a test set of trials without odors. When using a global neuronal population merging all recording sessions for this analysis (as in **Fig. 6c**), the classifier score for discrimination was 100% in both cases, suggesting no strong impact of odors on tactile coding. For a more sensitive measurement, we also performed this analysis on single sessions (local populations). In this case again, we found no systematic difference between the classification scores obtained in the presence and the absence of odor (**Fig. 6e**), confirming that odor-

evoked activity does not strongly modify tactile representations along dimensions that are important for their discrimination (**Fig. 6f**). As suggested previously[32,33], independence of two representations suggests that they are contained in orthogonal spaces. To verify this for olfactory and tactile representations in barrel cortex, we measured the dot product between the vector separating the mean representations of the two odors and the vector separating the representation of the two grating orientations. The dot product was close to zero throughout time (**Fig. 6g, h**) indicating that odor and tactile decoding axes are orthogonal. This shows that, in our experimental conditions, olfactory and tactile information are encoded in orthogonal subspaces of barrel cortex population activity.

# Discussion

Using 2-photon calcium imaging during olfactory-tactile stimulation in head-fixed mice with an intact whisker pad, we observed that barrel cortex encodes information about odor identity in parallel with the tactile representations of the proximal environment. We identify two mechanisms for odor-induced modulations of barrel cortex activity: a peripheral one, related to altered whisking when an odor is present (**Fig. 2-3**), and another, presumably of central origin, that is independent of whisking and cholinergic signalling (**Fig. 4-5**). Together, these two mechanisms affect about one fifth of stimulus-responsive barrel cortex neurons in freely whisking animals, while the latter, central mechanism impacts only about one tenth of the stimulus-responsive neurons. Despite this modest proportion, whisking-independent odor representations are sufficient to reliably decode not only the presence of an odor, but also its identity, making it unlikely that these modulations reflect intact efference copies of whisking programs after facial nerve sectioning (**Fig. 6**). In turn, it is unclear whether whisking-dependent effects themselves inform about odor identity as they could not be disentangled from the whisking-independent effects. However, odor decoding was not significantly improved when mice could whisk (**Supplementary Fig. 3**). Moreover, the relevance of whisking-dependent effects for behavior is difficult to interpret. In our experimental conditions, they reflect global changes in the dynamics of the whisker pad which most probably corresponds to an increase in the engagement of the animal to explore its near environment whether it contacts an object or not (**Fig. 3**). Although these reafferent signals impact barrel cortex, it is possible that they are compensated by efference copies from motor centers [34–36]. In a goal-directed context, these effects may also be cancelled by a tighter control of whisking during behavior [37,38].

Whisking-independent effects may reflect in contrast a more central cross-modal signaling mechanism. Our pharmacological manipulations (**Fig. 5 and Supplementary Fig. 4**) show that they do not depend on cholinergic signaling, indicating that they do not reflect attentional modulation mediated by this pathway. This does not rule out signaling by other neuromodulatory pathways which could play a role as suggested by the fact that both whisking and breathing are affected by the presence of an odor in our experimental conditions[39–42]. For these effects to be entirely driven by neuromodulatory signaling, it would mean that neuromodulatory inputs to barrel cortex are odor-identity specific, as amyl acetate and ethyl butyrate trials can be discriminated based on barrel cortex activity (**Fig. 6 and Supplementary Fig. 3**).

Outside of neuromodulatory sources, there are several other pathways that could introduce odor information into barrel cortex representation. Although there are no direct inputs to barrel cortex from the piriform cortex[12,43], they are bidirectionally connected to common associative areas, in particular the perirhinal cortex[12,44–47]. The perirhinal cortex, which is located just above the piriform cortex on the ventro-dorsal axis, is an associative area that has been implicated in multimodal object recognition[48–51]. To the best of our knowledge, no study has addressed its potential role in olfactory-tactile integration, but in the rodent, it could be a multimodal hub that combines these two sensory modalities among others. In this case, the odor-evoked activity we observe in barrel cortex would represent feedback information from an associative area. Alternatively, barrel cortex receives inputs from several thalamic nuclei, including from secondary thalamic regions which themselves are known to receive multimodal inputs[52].

Independent of the pathway mediating it, the functional significance of olfactory signaling in barrel cortex remains an open question. We observed that olfactory activity in barrel cortex contains an equal amount of inhibitory and excitatory responses and builds neural representations orthogonal to tactile representations. Hence, for the odors and gratings that we presented in a naive behavioral context, information from the two modalities does not bias each other at barrel cortex level. Coincident olfacto-tactile stimulations neither sharpen tactile representations in barrel cortex as has been observed recently in the visual cortex with sounds[14,15], nor do they improve detection of multimodal coincidence. The advantage of this coding scheme is that barrel cortex can access olfactory information without perturbations of the tactile code. However, the presence of olfactory information in barrel cortex could enable the emergence of cross-modal associations, in specific behavioral contexts which require information from both modalities[53]. The fact that odors have both inhibitory and excitatory effects (**Figs. 2 and 4**) suggests that odors could suppress some aspects of the tactile representations and boost others, but such mechanisms would not be engaged in the absence of specific associations.

Together our results demonstrate a novel site of convergence for olfactory and tactile information early in the sensory processing hierarchy and open interesting avenues to study the role of brain wide interactions in processing two sensory modalities that are crucial in rodents' daily life.

# Methods

### Cranial window implantation and viral injections.

All procedures were conducted in accordance with protocols approved by the French Ethical Committee (authorization 00275.01). We used 8 to 12-weeks-old C57BL/6J mice housed 1-4 per cage, in normal light/dark cycle (12h/12h). Cranial window implantation and viral injections were performed under isoflurane anesthesia (1.3-1.7%) with body temperature maintained constant at 37°C using a regulated thermal blanket with a rectal probe (Rodent Warmer X1, Stoelting). A craniotomy of 4 mm in diameter was drilled over the barrel cortex on the left hemisphere. Four injections of 200 nl of AAV1-syn-GCaMP6s ($1x10^{-12}$ $vg.ml^{-1}$) obtained from Vector Core (Philadelphia, PA, USA) with glass micropipettes and a programmable pump (Micro 4; World Precision Instruments) at 30 $nl.min^{-1}$ around the C2 barrel column at

AP -1.6, ML -3.3, DV 0.5[19]. The craniotomy was sealed with a glass window comprising two circular coverslips bound together with optical glue (5 and 3 mm diameter) and a metal post for head-fixation was implanted using dental cement (Super-Bond C&B, Sun Medical Co. Ltd.).

### Facial nerve transection

For experiments in the passive context, whisking was prevented by bilateral sectioning of the inferior and superior buccal branches of the facial nerve[54]. Mice were anesthetized under isoflurane with their temperature monitored as for cranial window implantation. A small 3 mm cut of the skin was performed to expose the buccal branches of the facial nerve which were sectioned with microsurgical scissors. The cut was then closed with a nylon suture.

### Intrinsic optical imaging

The location of the GCaMP6s expression locus in barrel cortex was validated with intrinsic optical imaging under isoflurane anesthesia (1%;  SomnoSuite, Kent Scientific) on a thermal blanket. The signal was obtained under 625 nm LED illumination and images of the vasculature over the same field of view were taken under 480 nm LED illumination. Reflected light was acquired with a CCD camera (GC651MP, Smartek Vision) equipped with a 50 mm objective (Fujinon, HF50HA-1B, Fujifilm) on a 656 x 496 pixel region and resolution of 5.58 µm per pixel at 15 fps through a cranial window 1 to 2 weeks after implantation. Four seconds after imaging onset, the C2 whisker was deflected by a piezoelectric bender (PI PICMA Bender) at 10 Hz for 4 sec following a sinusoidal wave along the rostrocaudal axis, for twenty trials with 8 sec inter-trial intervals. Change in reflectance was computed as $(R_{stim} - R_{base}) / R_{base}$ where $R_{stim}$ and $R_{base}$ are averaged over the 4 sec of stimulus presentation and baseline, respectively. Response images were averaged across all deflections. Mice whose intrinsic response did not coincide with the GCaMP6s expression locus were excluded from further analysis.

### Odor delivery and grating presentation

Odors (amyl acetate and ethyl butyrate) were from Sigma-Aldrich and delivered with a custom-made olfactometer (**Supplementary Fig. 1**). Mass flow controllers were used to pass air flow through small bottles (Wilmad ML-1490-702, SP Scienceware) filled with 20 ml of odor solution diluted at 0.1% in mineral oil. The total flow was constant (1 $l.min^{-1}$) and the snout of the animal was placed inside a confined air stream to prevent movement of the whiskers. To obtain a stable concentration during stimulus application, we ensured that the flow was stationary with a 5 sec bubbling period before the stimulus was presented. Photoionization detector measurements were made (**Supplementary Fig. 1**) to precisely synchronize the timing of arrival of the odorized air flow to the snout with the final position of the grating (active context) or the onset of the sweep (passive context).

Orientated gratings were made of five ridges of 3.5 mm thickness and spacing on a 3d printed PLA disk of 35 mm diameter. Gratings were brought to the animal or swept using a custom-made presentation

wheel consisting of two stepper motors (42BYG, Makeblock) mounted on a linear stage (eTrack, Newmark) and controlled with an Arduino.

All parts of the stimulation system were timed and synchronized with a data acquisition card (USB-6343-BNC, National Instruments) and MATLAB scripts (Mathworks). Bimodal conditions were presented 10 times (40 total), unimodal conditions 20 times (80 total), and the blanks 30 times, for a total 150 pseudo-randomized trials with one stimulus presentation every 19 sec.

### Two-photon calcium imaging in awake mice

One week before imaging, mice were trained to stand still, head-fixed under the microscope for five consecutive days for 15 min to 1 h per day. Then mice were imaged for 1h long sessions with up to four vertical depths imaged per mouse on different days. Imaging was performed using a two-photon microscope (Femtonics, Budapest, Hungary) equipped with an 8 kHz resonant scanner combined with a pulsed laser (MaiTai-DS, SpectraPhysics, Santa Clara, CA, USA) tuned at 920 nm. The objective was a 10x Olympus (XLPLN10XSVMP), obtaining a field of view of 1000 x 1000 µm. Images were acquired at 31.5 Hz during blocks of 11 sec interleaved with 8 sec intervals.

### Calcium imaging data analysis

Data analysis was performed using Python scripts. Motion artifacts, regions of interest selection, and the signal extraction was carried out using Suite2p [55]. Neuropil contamination was subtracted by applying the following equation: $F_{cor}(t) = F(t) - 0.7\ F_n(t)$. Then the change in fluorescence $\Delta F/F_0$ was calculated as $(F_{cor}(t) - F_0) / F_0$, where $F_0$ is estimated as the 8th percentile of F for each trial. To account for baseline fluctuations, the baseline activity two to one seconds before stimulus onset was subtracted for all cells on each trial. In total, 9714 neurons were recorded from 12 mice over 20 sessions in the active condition, and 14408 neurons from 6 mice over 19 sessions in the passive condition. Among those populations, 1907 (19.6%) and 5162 (35%) neurons in the active and passive contexts, respectively, were responsive to at least one of the nine stimulation conditions (significance level = 5%; Kruskal-Wallis test) and were kept for analysis. Single cell ΔF/F averages were computed over the 2 sec of stimulus presentation and were considered odor responsive if their mean response was significantly different in the comparison between bimodal trials with grating only trials or odor only trials with blanks. For simplicity, we first evaluated the modulation by grouping together trials with odors, regardless of odor identity, resulting in four condition categories (bimodal, grating only, odor only, and blank; **Figs. 2-4**). We defined the olfactory modulation index as $(\Delta F/F_{odor} - \Delta F/F_{no\ odor}) / \Delta F/F_{no\ odor}$ with $\Delta F/F_{odor}$ and $\Delta F/F_{no\ odor}$ the average response over stimulus presentation to bimodal and grating only conditions or odor only and blank, respectively [56].

### Whisker tracking and breathing monitoring

The full whisker pad was monitored with a high-speed camera (HXC20, Baumer) at 500 Hz and 608 x 600 pixels per frame under infrared backlight. Automated tracing of the whiskers and extraction of angle and curvature was performed with Whisk[20]. For each frame, angles and curvatures of detected whiskers (~12

per frame) were averaged to obtain a global measurement for the whisker pad. The phase of the whisking cycle was computed by applying a Hilbert transform to the band-pass filtered azimuthal angle ($2^{nd}$ order butterworth filter, 4-30 Hz) from which the time point of maximum protraction and retraction were retrieved [34]. Amplitude and setpoint were then defined as the range and center of angular motion over a single cycle after quadratic interpolation. Absolute change in curvature was obtained by taking the absolute curvature and subtracting a baseline defined as the average absolute curvature two to one sec before stimulus presentation.

Breathing was monitored with a microbridge mass airflow sensor (Honeywell AWM3300V, Morris Plains, NJ) positioned in front of the animal's snout and perpendicular to the air stream [57]. Negative change in voltage corresponds to inhalation. Traces were sampled at 1 kHz and bandpass filtered ($2^{nd}$ order butterworth filter, 4-20 Hz) and a Hilbert transform was used similarly to obtain breathing amplitude similarly to whisking. Breathing frequencies over a 2 sec duration before and after stimulus presentation were defined as the peak in the power spectrum computed with Welch's method.

### Silencing of cholinergic inputs

For pharmacological manipulation of cholinergic signaling, 400 nl of 1 mM atropine and mecamylamine was injected into barrel cortex via a hole through the cranial window while the animal was awake. To allow for diffusion, we waited 30 min after injection before starting the recording. Controls were performed by injection of 400 nl of saline. Control and silencing recordings were made with a two days interval starting with controls first for half the experiments and silencing first for the other half. A similar plane was imaged in control and silencing sessions but the identity of cells were not tracked across sessions.

### Stimulus decoding and orthogonality

To evaluate the robustness of odor-evoked activity in barrel cortex, we tested the accuracy at which the presented stimulus could be decoded from single-trial population responses by training and testing a nearest centroid classifier with a stratified k-fold cross-validation procedure implemented in Scikit-learn. Single-trial global population vectors were constructed with neurons recorded from all sessions using ΔF/F averages in 1 sec time bins. Training and testing sets were created by randomly partitioning single trials in k = 10 pairwise disjoint groups with equal number of trials from the two tested conditions, each serving as a test set against the others. This procedure was repeated 10 times and the accuracy of the classification was defined at the average of these 10 cross-validations. To evaluate its significance, the same procedure was performed for n = 1000 shuffles of the conditions and the accuracy of the non-shuffled data was located in the distribution of shuffled accuracies to obtain a p-value. Note that the precision of the p-value was limited to 3 decimals as 1000 shuffles were performed. For decoding between sessions (**Supplementary Fig. 3**), population vectors were constructed with neurons recorded in single sessions using ΔF/F averages in 1 sec time bins. The same k-fold cross-validation procedure was applied. Each session was used to obtain a cross-validated accuracy with and without shuffling.

Significance was assessed by comparing the mean accuracy of the real and shuffled data (Wilcoxon signed-rank test). The data was z-scored to reach significance in the results presented in **Supplementary Fig. 3**, in accordance with the usual machine learning prerequisite for classification: the average response of each cell to all conditions of stimulus presentation was subtracted and scaled by the standard deviation over the same epoch.

To study the independence of the tactile and olfactory information, we considered the decoding axes classifying grating orientation and odor identity (**Fig. 6c, d**), defined as the difference vectors between the corresponding conditions, which we projected onto each other (**Fig. 6h**). Specifically, we took the olfactory decoding axis that we projected across time onto the tactile decoding axis defined on the second time bin after stimulus presentation (during which olfactory information is maximal), we then took the norm of the resulting projection as our measure of orthogonality.

### Statistical analysis

All quantification and statistical analysis were performed with Python scripts. Plotting relied on Matplotlib and Seaborn. Statistical assessment was performed with non-parametric tests implemented in the Statistical functions module reported in figures and legends together with mean and 95% confidence interval, the number of samples used for the test and the nature of the samples (number of sessions for between sessions assessment and number of trials for within sessions assessment). Hypotheses were two-sided and significance levels were set at 5%. Confidence intervals were computed by the bootstrap procedure implemented in Seaborn with n = 1000 bootstrap iterations. In all analyses, all subjects which underwent a particular protocol in the study were included.

# Declarations

### Data and code availability

The data that support the findings of this study and the analysis code are available from the corresponding author upon reasonable request.

### Acknowledgements

We thank Sophie Bagur for helpful comments on the manuscript. This work was supported by the Fondation pour la Recherche Médicale (FRM grant number ECO20170637482 to A.R.), the International Human Frontier Science Program Organization (CDA-0064-2015), the European Research Council (ERC CoG 770841) and the Paris-Saclay University.

### Author contributions

A.R. and B.B. performed the experiments, A.R. and E.H constructed the stimulators, A.R. analysed the data, A.R., E.H., B.B. designed the study and wrote the manuscript.

### Declaration of interests

We declare no conflict of interests.

# References


1. Stein, B. E. & Stanford, T. R. Multisensory integration: current issues from the perspective of the single neuron. *Nat Rev Neurosci* **9**, 255–66 (2008).
2. Alais, D. & Burr, D. The ventriloquist effect results from near-optimal bimodal integration. *Curr Biol* **14**, 257–62 (2004).
3. Botvinick, M. & Cohen, J. Rubber hands 'feel' touch that eyes see. *Nature* **391**, 756 (1998).
4. McGurk, H. & MacDonald, J. Hearing lips and seeing voices. *Nature* **264**, 746–8 (1976).
5. Ernst, M. O. & Banks, M. S. Humans integrate visual and haptic information in a statistically optimal fashion. *Nature* **415**, 429–33 (2002).
6. Gu, Y., Angelaki, D. E. & Deangelis, G. C. Neural correlates of multisensory cue integration in macaque MSTd. *Nat Neurosci* **11**, 1201–10 (2008).
7. Fetsch, C. R., Pouget, A., DeAngelis, G. C. & Angelaki, D. E. Neural correlates of reliability-based cue weighting during multisensory integration. *Nat Neurosci* **15**, 146–54 (2012).
8. Raposo, D., Kaufman, M. T. & Churchland, A. K. A category-free neural population supports evolving demands during decision-making. *Nat Neurosci* **17**, 1784–92 (2014).
9. Raposo, D., Sheppard, J. P., Schrater, P. R. & Churchland, A. K. Multisensory Decision-Making in Rats and Humans. *J. Neurosci.* **32**, 3726–3735 (2012).
10. Nikbakht, N., Tafreshiha, A., Zoccolan, D. & Diamond, M. E. Supralinear and Supramodal Integration of Visual and Tactile Signals in Rats: Psychophysics and Neuronal Mechanisms. *Neuron* **97**, 626-639.e8 (2018).
11. Cappe, C., Rouiller, E. M. & Barone, P. Multisensory anatomical pathways. *Hear Res* **258**, 28–36 (2009).
12. Zingg, B. *et al.* Neural Networks of the Mouse Neocortex. *Cell* **156**, 1096–1111 (2014).
13. Iurilli, G. *et al.* Sound-driven synaptic inhibition in primary visual cortex. *Neuron* **73**, 814–28 (2012).
14. Ibrahim, L. A. *et al.* Cross-Modality Sharpening of Visual Cortical Processing through Layer-1-Mediated Inhibition and Disinhibition. *Neuron* **89**, 1031–45 (2016).
15. Deneux, T. *et al.* Context-dependent signaling of coincident auditory and visual events in primary visual cortex. *Elife* **8**, (2019).
16. Moore, J. D. *et al.* Hierarchy of orofacial rhythms revealed through whisking and breathing. *Nature* **497**, 205–10 (2013).
17. Boisselier, L., Ferry, B. & Gervais, R. Involvement of the lateral entorhinal cortex for the formation of cross-modal olfactory-tactile associations in the rat. *Hippocampus* **24**, 877–891 (2014).

18. Ito, J. *et al.* Whisker barrel cortex delta oscillations and gamma power in the awake mouse are linked to respiration. *Nat. Commun.* **5**, (2014).
19. Knutsen, P. M., Mateo, C. & Kleinfeld, D. Precision mapping of the vibrissa representation within murine primary somatosensory cortex. *Philos. Trans. R. Soc. B Biol. Sci.* **371**, (2016).
20. Clack, N. G. *et al.* Automated Tracking of Whiskers in Videos of Head Fixed Rodents. *PLOS Comput. Biol.* **8**, e1002591 (2012).
21. Urbain, N. *et al.* Whisking-Related Changes in Neuronal Firing and Membrane Potential Dynamics in the Somatosensory Thalamus of Awake Mice. *Cell Rep.* **13**, 647–656 (2015).
22. Chakrabarti, S. & Schwarz, C. Cortical modulation of sensory flow during active touch in the rat whisker system. *Nat. Commun.* **9**, (2018).
23. Gil, Z., Connors, B. W. & Amitai, Y. Differential Regulation of Neocortical Synapses by Neuromodulators and Activity. *Neuron* **19**, 679–686 (1997).
24. Oldford, E. & Castro-Alamancos, M. Input-specific effects of acetylcholine on sensory and intracortical evoked responses in the “barrel cortex” in vivo. *Neuroscience* (2003) doi:10.1016/S0306-4522(02)00663-2.
25. Gulledge, A. T. & Stuart, G. J. Cholinergic Inhibition of Neocortical Pyramidal Neurons. *J. Neurosci.* **25**, 10308–10320 (2005).
26. Eggermann, E., Kremer, Y., Crochet, S. & Petersen, C. C. H. Cholinergic Signals in Mouse Barrel Cortex during Active Whisker Sensing. *Cell Rep.* **9**, 1654–1660 (2014).
27. Kuchibhotla, K. V. *et al.* Parallel processing by cortical inhibition enables context-dependent behavior. *Nat. Neurosci.* **20**, 62–71 (2017).
28. Herrero, J. L. *et al.* Acetylcholine contributes through muscarinic receptors to attentional modulation in V1. *Nature* **454**, 1110–1114 (2008).
29. Parikh, V., Kozak, R., Martinez, V. & Sarter, M. Prefrontal Acetylcholine Release Controls Cue Detection on Multiple Timescales. *Neuron* **56**, 141–154 (2007).
30. Buzsaki, G. *et al.* Nucleus basalis and thalamic control of neocortical activity in the freely moving rat. *J. Neurosci.* **8**, 4007–4026 (1988).
31. Bathellier, B., Buhl, D. L., Accolla, R. & Carleton, A. Dynamic ensemble odor coding in the mammalian olfactory bulb: sensory information at different timescales. *Neuron* **57**, 586–598 (2008).
32. Kaufman, M. T., Churchland, M. M., Ryu, S. I. & Shenoy, K. V. Cortical activity in the null space: permitting preparation without movement. *Nat. Neurosci.* **17**, 440–448 (2014).
33. Bagur, S. *et al.* Go/No-Go task engagement enhances population representation of target stimuli in primary auditory cortex. *Nat. Commun.* **9**, 2529 (2018).
34. Hill, D. N., Curtis, J. C., Moore, J. D. & Kleinfeld, D. Primary Motor Cortex Reports Efferent Control of Vibrissa Motion on Multiple Timescales. *Neuron* **72**, 344–356 (2011).
35. Fee, M. S., Mitra, P. P. & Kleinfeld, D. Central Versus Peripheral Determinants of Patterned Spike Activity in Rat Vibrissa Cortex During Whisking. *J. Neurophysiol.* **78**, 1144–1149 (1997).

36. Bell, C. C. An efference copy which is modified by reafferent input. *Science* **214**, 450–453 (1981).
37. Chen, J. L., Carta, S., Soldado-Magraner, J., Schneider, B. L. & Helmchen, F. Behaviour-dependent recruitment of long-range projection neurons in somatosensory cortex. *Nature* **499**, 336–340 (2013).
38. Chen, J. L. *et al.* Pathway-specific reorganization of projection neurons in somatosensory cortex during learning. *Nat. Neurosci.* **18**, 1101–1108 (2015).
39. Constantinople, C. M. & Bruno, R. M. Effects and Mechanisms of Wakefulness on Local Cortical Networks. *Neuron* **69**, 1061–1068 (2011).
40. Hattox, A., Li, Y. & Keller, A. Serotonin Regulates Rhythmic Whisking. *Neuron* **39**, 343–352 (2003).
41. Hirata, A., Aguilar, J. & Castro-Alamancos, M. A. Noradrenergic Activation Amplifies Bottom-Up and Top-Down Signal-to-Noise Ratios in Sensory Thalamus. *J. Neurosci.* **26**, 4426–4436 (2006).
42. Hong, E. Y., Beak, S. K. & Lee, H. S. Dual projections of tuberomammillary neurons to whisker-related, sensory and motor regions of the rat. *Brain Res.* **1354**, 64–73 (2010).
43. Oh, S. W. *et al.* A mesoscale connectome of the mouse brain. *Nature* **508**, 207–214 (2014).
44. Aronoff, R. *et al.* Long-range connectivity of mouse primary somatosensory barrel cortex. *Eur. J. Neurosci.* **31**, 2221–2233 (2010).
45. Zakiewicz, I. M., Bjaalie, J. G. & Leergaard, T. B. Brain-wide map of efferent projections from rat barrel cortex. *Front. Neuroinformatics* **8**, (2014).
46. Fabri, M. & Burton, H. Ipsilateral cortical connections of primary somatic sensory cortex in rats. *J. Comp. Neurol.* **311**, 405–424 (1991).
47. Naber, P. A., Witter, M. P. & Lopes da Silva, F. H. Differential distribution of barrel or visual cortex. Evoked responses along the rostro-caudal axis of the peri- and postrhinal cortices. *Brain Res.* **877**, 298–305 (2000).
48. Doan, T. P., Lagartos-Donate, M. J., Nilssen, E. S., Ohara, S. & Witter, M. P. Convergent Projections from Perirhinal and Postrhinal Cortices Suggest a Multisensory Nature of Lateral, but Not Medial, Entorhinal Cortex. *Cell Rep.* **29**, 617-627.e7 (2019).
49. Xiang, J. Z. & Brown, M. W. Differential neuronal encoding of novelty, familiarity and recency in regions of the anterior temporal lobe. *Neuropharmacology* **37**, 657–676 (1998).
50. Meunier, M., Bachevalier, J., Mishkin, M. & Murray, E. A. Effects on visual recognition of combined and separate ablations of the entorhinal and perirhinal cortex in rhesus monkeys. *J. Neurosci. Off. J. Soc. Neurosci.* **13**, 5418–5432 (1993).
51. Brown, M. W., Wilson, F. A. W. & Riches, I. P. Neuronal evidence that inferomedial temporal cortex is more important than hippocampus in certain processes underlying recognition memory. *Brain Res.* **409**, 158–162 (1987).
52. Cappe, C., Morel, A., Barone, P. & Rouiller, E. M. The thalamocortical projection systems in primate: an anatomical support for multisensory and sensorimotor interplay. *Cereb Cortex* **19**, 2025–37 (2009).
53. Bobrov, E., Wolfe, J., Rao, R. P. & Brecht, M. The representation of social facial touch in rat barrel cortex. *Curr. Biol. CB* **24**, 109–115 (2014).

54. Dörfl, J. The innervation of the mystacial region of the white mouse. *J. Anat.* **142**, 173–184 (1985).
55. Pachitariu, M. *et al.* Suite2p: beyond 10,000 neurons with standard two-photon microscopy. *bioRxiv* 061507 (2017) doi:10.1101/061507.
56. Stein, B. E., Stanford, T. R., Ramachandran, R., Perrault, T. J. & Rowland, B. A. Challenges in Quantifying Multisensory Integration: Alternative Criteria, Models, and Inverse Effectiveness. *Exp. Brain Res. Exp. Hirnforsch. Exp. Cerebrale* **198**, 113–126 (2009).
57. Bolding, K. A. & Franks, K. M. Complementary codes for odor identity and intensity in olfactory cortex. *eLife* (2017) doi:10.7554/eLife.22630.

# Figures

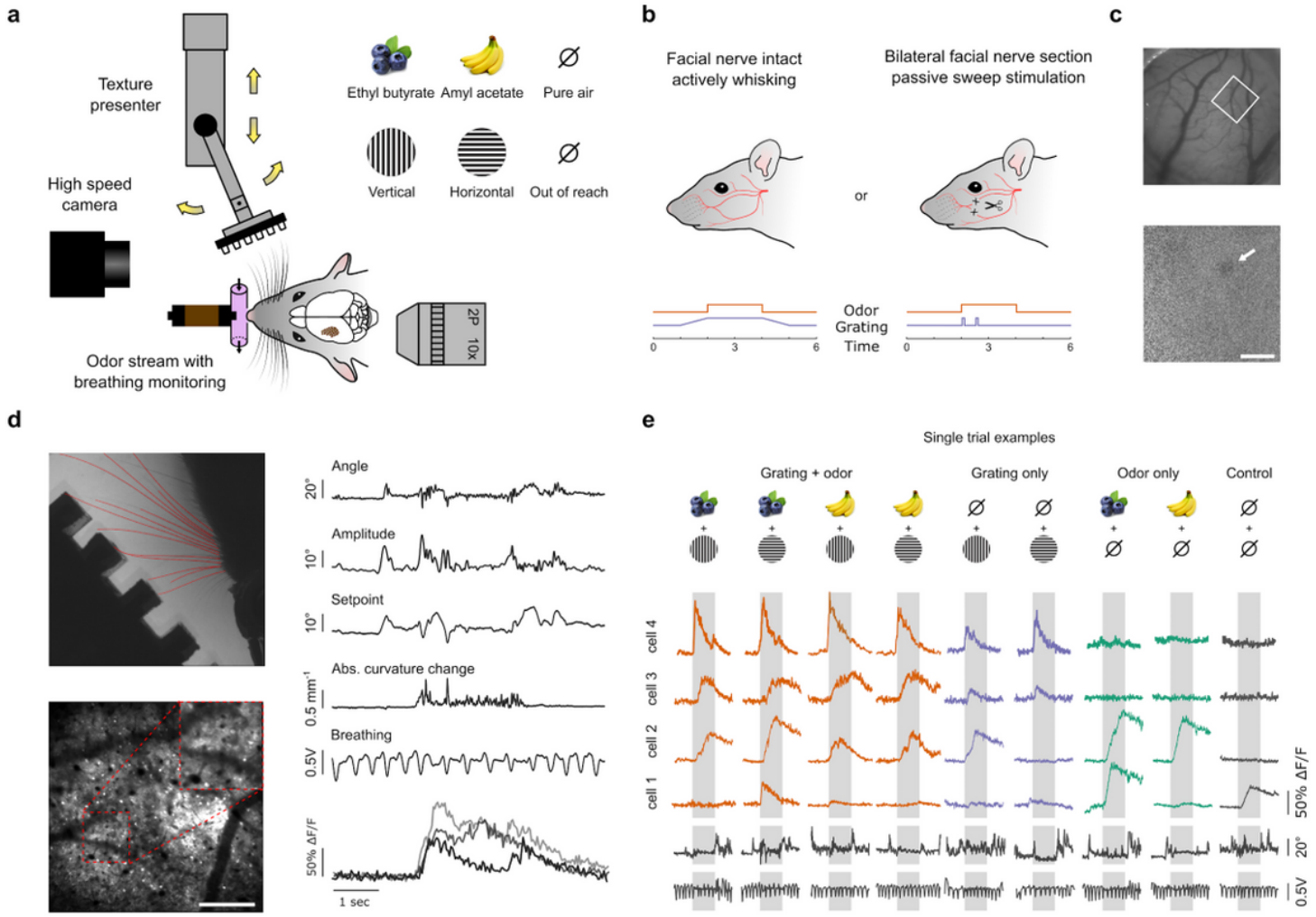


## Figure 1

Calcium imaging in L2/3 of mouse barrel cortex during olfacto-tactile stimulation. a Schematic of olfacto-tactile stimulation setup. A grating was moved in contact with the whiskers in either the vertical or horizontal orientation, while ethyl butyrate or amyl acetate was presented through a constant air stream.

Whisking was recorded with high-speed videography (500Hz) and breathing was monitored with a pressure sensor. b Schematics of the two recording conditions. Left: facial nerve intact, mice whisked freely on the grating brought to their whiskers together with stimulation timing. Right: facial nerve sectioned, the grating was swept on the whiskers while whisking was abolished. c Example of C2 barrel localization with intrinsic signal imaging used to confirm the location of GCaMP6s expression in barrel cortex (scale bar: 1 mm, white square: two photon field of view, arrow: C2 response). d Top left: tracking of average whisker pad position and curvature. Bottom left: image of in vivo GCaMP6s expression in L2/3 (scale bar: 250 µm). Right: example of simultaneously recorded whisker pad kinematics, breathing, and raw ΔF/F0 traces. Dashed lines indicate onset and offset of grating approach; gray shading indicates epoch of stimulation during which odors were present in the air stream. e Illustration of the nine combinations of tactile and olfactory stimuli with single trial example ΔF/F0 traces from four neurons showing olfactory responses.

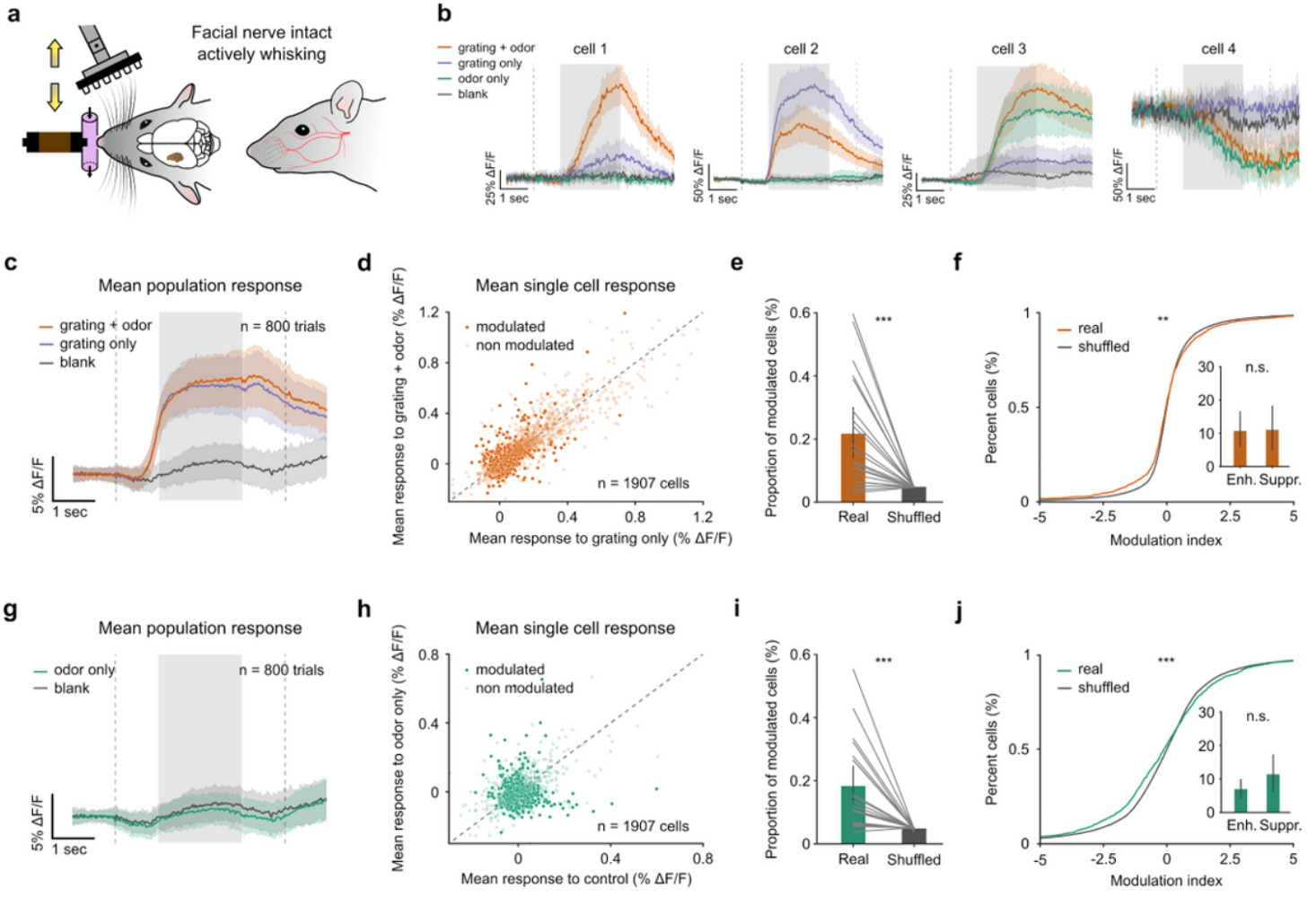


## Figure 2

Odor-induced responses of L2/3 barrel cortex cells in active stimulation context. a Schematic of the stimulation condition with facial nerve intact. Gratings were brought in contact with the whiskers. b Average ΔF/F for four example neurons displaying diverse odor responses. c-f Responses to grating+odor stimulation compared with grating only. Stimuli were grouped into four categories: grating+odor (orange),

grating only (blue), odor only (green), and control (gray). c Population averages to grating+odor trials (both orientations and both odors grouped together; orange) and grating only trials (both grating orientations grouped together; blue); average to blank (gray) is shown for comparison . d Scatter plot of mean ΔF/F to grating+odor versus grating only for 1907 neurons. Neurons plotted in dark were significantly modulated ($p < 0.05$, Mann-Whitney U test). Dashed line indicates diagonal. e Proportion of modulated neurons across sessions compared with shuffled conditions (21.71% (14.69, 29.58) for real data; 4.84% (4.80, 4.87) for shuffled data; p = 2x10-5; Wilcoxon signed-rank test). f Cumulative distribution of modulation index for grating+odor versus grating alone (p = 0.109; Kolmogorov-Smirnov test). Inset: proportion of enhanced and suppressed cells (mean enhanced = 10.35% (5.60, 15.77); mean suppressed = 11.36% (6.06, 17.60); p = 0.793; Wilcoxon signed-rank test). g-j Response to olfactory stimulations alone compared with control. g Population averages to odor only trials (green) and control (gray) (mean of odors only trials = 0.57% ΔF/F (-0.64, 2.01), mean of blank trials = 1% ΔF/F (0.28, 1.81) computed over stimulation epoch; p = 0.394; n = 800 trials from 20 sessions; Mann-Whitney U test). h Analog to d. i Analog to e (18.34% (12.78, 24.76) for real data; 4.89% (4.84, 4.94) for shuffled data; p = 1x10-5; Wilcoxon signed-rank test). j Analog to f (p = 2.3x10-4; Kolmogorov-Smirnov test; inlet: mean enhanced = 6.97% (4.48, 9.98); mean suppressed = 11.36% (6.10, 17.52); p = 0.398; Wilcoxon signed-rank test).

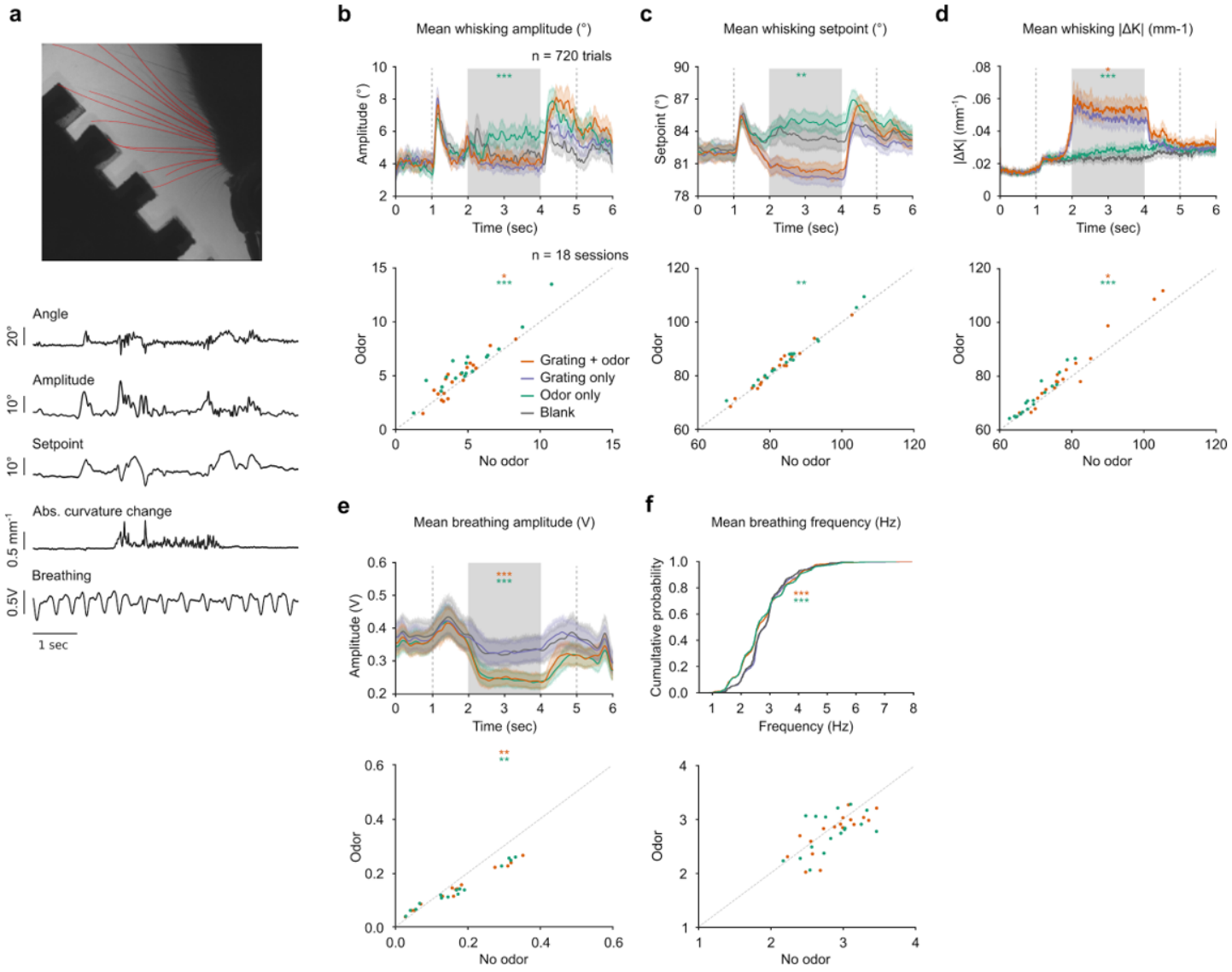


## Figure 3

Olfactory stimulations decrease breathing and increase whisking kinematics. a Example image of whisker pad tracking with traces of derived whisking kinematic parameters and breathing signal shown below. b Top: mean whisking amplitude within sessions. Bottom: mean whisking amplitude between sessions. Whisking was analysed over the 2 sec stimulation epoch indicated by gray shading (orange: bimodal versus grating only; green: odor alone versus blank). c Top: mean setpoint within sessions. Bottom: mean setpoint between sessions. d Mean absolute curvature change within sessions. Bottom: mean absolute curvature change between sessions. e Mean breathing amplitude within sessions. Bottom: mean breathing amplitude between sessions. f Cumulative distribution of breathing frequency within sessions. Bottom: mean breathing frequency between sessions. n = 18 sessions from 10 mice; *p<0.05, **p<0.01, ***p<0.001; Wilcoxon signed-rank test; see Supplementary Table 1 and 2 for detailed statistics.

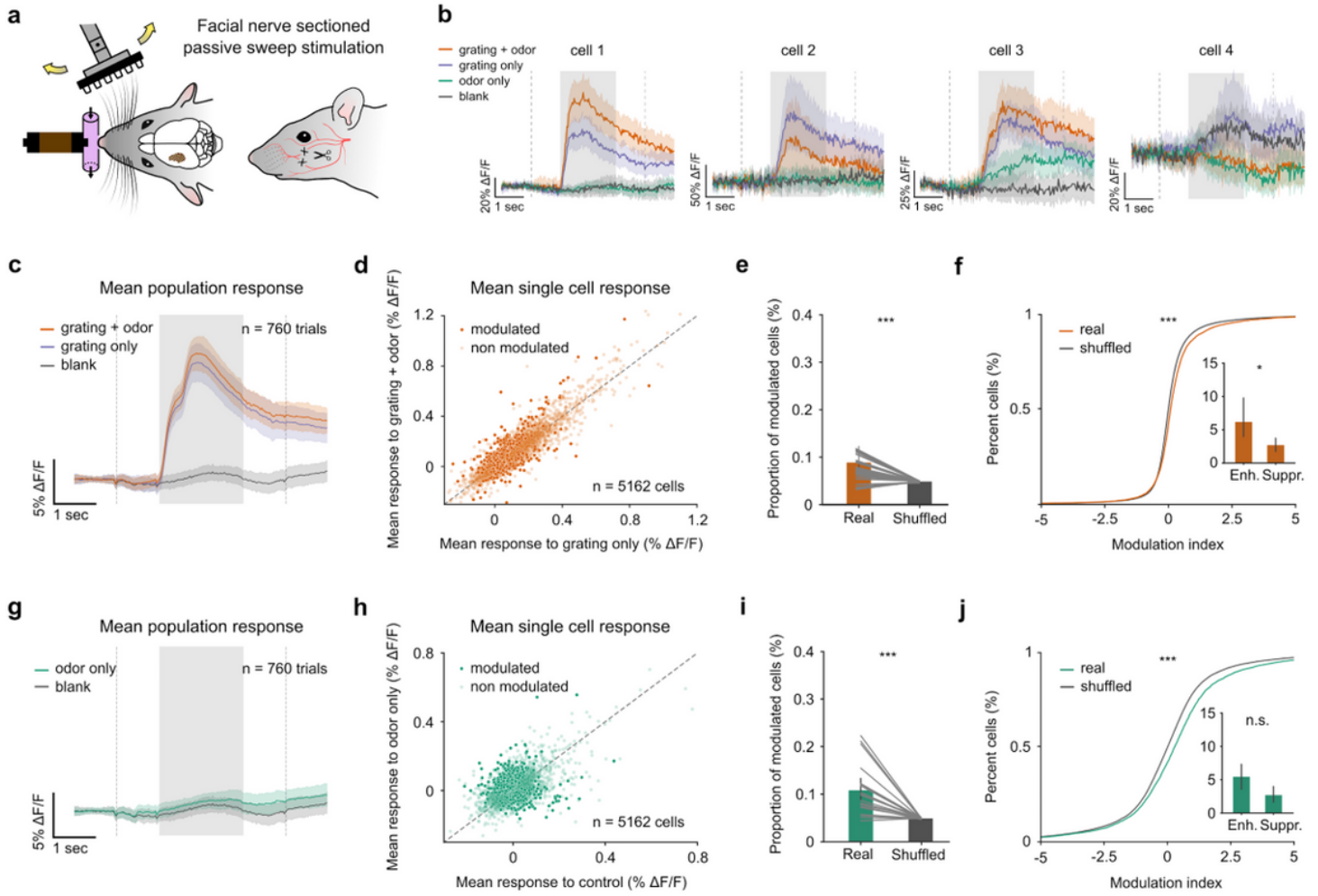


## Figure 4

Odor-induced activity in barrel cortex persists in the absence of whisking. a Schematic of the stimulation context with facial nerve sectioned. Gratings were brushed against the whiskers in a back and forth sweep. b-j As in Fig. 1, b-j. b Average ΔF/F for four example neurons displaying diverse odor responses. c Population averages to grating+odor trials (orange) and grating only trials (blue); average to control (gray) is shown for comparison (mean of bimodal trials = 11.22% ΔF/F (10.78, 11.66); mean of gratings only trials = 10.32% ΔF/F (9.81,10.73); p = 0.001 within sessions; n = 760 trials; Mann-Whitney U test; p = 0.28 between sessions; n = 19 sessions; Wilcoxon signed-rank test). d Scatter plot of mean ΔF/F to grating+odor versus grating only for 5162 neurons. Neurons plotted in dark are significantly modulated (p < 0.05, Mann-Whitney U test). Dashed line indicates diagonal. e Proportion of modulated neurons across sessions compared with shuffled conditions (8.99% (7.79, 10.57) for real data; 4.81% (4.75, 4.87) for shuffled data; p = 0.0006; Wilcoxon signed-rank test). f Cumulative distribution of modulation index for grating+odor versus grating alone (p = 1.15x10-17, Kolmogorov-Smirnov test). Inset: proportion of enhanced and suppressed cells (mean enhanced = 6.16% (3.89, 9.70); mean inhibited = 2.83% (1.68, 3.91); p = 0.047; n = 19 sessions; Wilcoxon signed-rank test). g Population averages to odor only trials (green) and control (gray) (mean of bimodal trials = 0.91% ΔF/F (0.62, 1.2); mean of gratings only trials = 0.29% ΔF/F (0, 0.61); p = 0.001 within sessions; n = 760 trials; Mann-Whitney U test; p = 0.25 between

sessions; n = 19 sessions; Wilcoxon signed-rank test). h Analog to d. i Analog to e (10.81% (8.55, 13.27) for real data; 4.89% (4.84, 4.94) for shuffled data; p = 0.0001; Wilcoxon signed-rank test). j Analog to f (p = 5.91x10-120; Kolmogorov-Smirnov test; inlet: mean enhanced = 7.24% (4.94, 9.84); mean suppressed = 3.57% (2.08, 5.26); p = 398; n = 19 sessions; Wilcoxon signed-rank test).

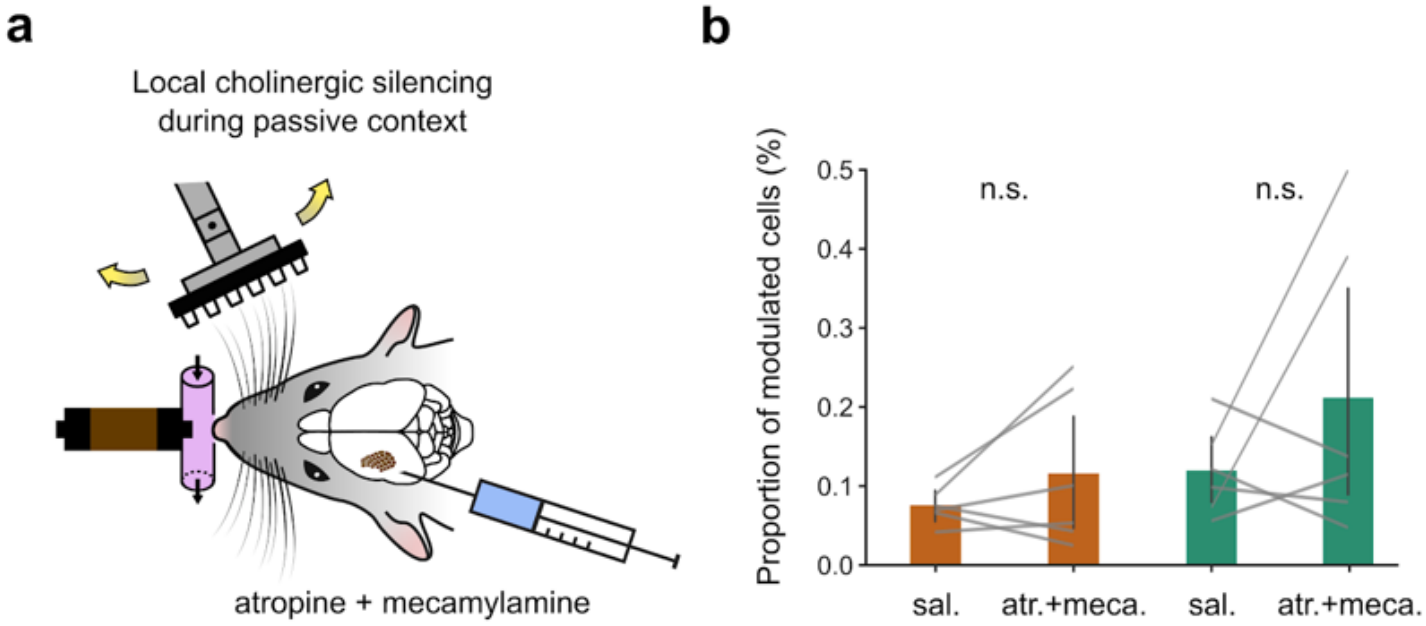


**Figure 5**

Pharmacological blockade of cholinergic transmission in barrel cortex does not reduce the proportion of olfactory modulated cells. a Schematics of local silencing of cholinergic transmission with 1mM injections of atropine (atr.) and mecamylamine (meca.) in barrel cortex during the passive stimulation context. b Proportion of modulated cells with and without unilateral cholinergic silencing (mean saline = 7.57% (5.93, 9.34); mean atr.+meca. = 11.59% (4.87, 18.63); p = 0.463; grating+odor versus grating only (orange); mean saline = 11.98% (8.17, 16.28); mean atr.+meca. = 21.24% (8.93, 35.75); p = 0.6; odor only versus blank (green); n = 12 sessions from 3 mice; Wilcoxon signed-rank test).

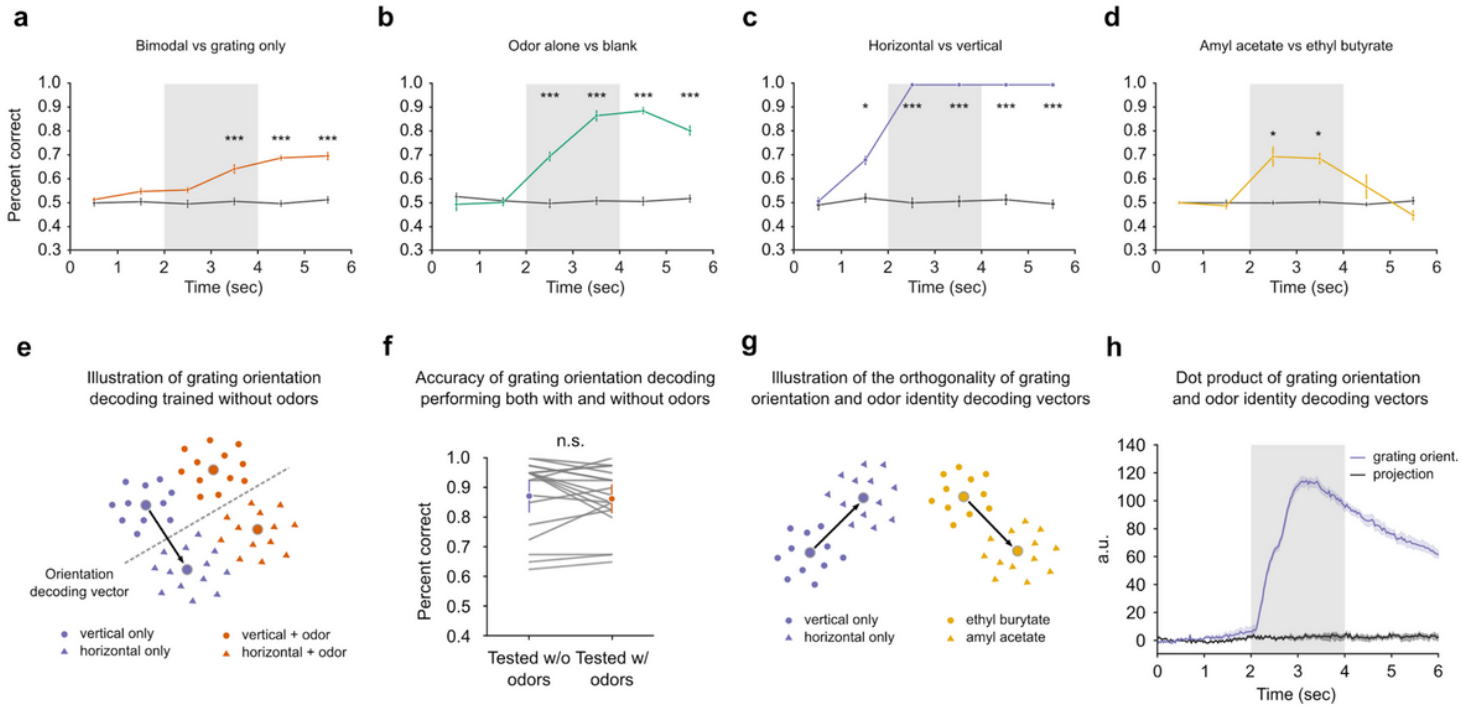


## Figure 6

Tactile and olfactory codes are independent in S1. a Accuracy of centroid classifiers decoding of grating orientation from S1 activity in the passive context averaged over 1 sec time bins. Performance for shuffled labels is shown in gray. P-values were obtained as the location of the mean accuracy in a distribution of 1000 shuffles; *p<0.05, **p<0.01, ***p<0.001. Error bars indicate 95% CI with n = 10 for real data and n = 100 for shuffled data; each data point is the average of a 20-fold stratified cross-validation; shading indicates stimulus presentation. b-d As in a for decoding of bimodal and grating only trials, odor only and blank, and odor identity, respectively. e Illustration of grating orientation decoding where the classifier was trained without odors but was able to separate the orientations when odors were present. The black arrow represents the decoding vector between the two classes of stimuli computed as the difference between the average population responses over stimulus presentation. f Accuracy of centroid classifiers trained to decode grating orientations without odors and showing no impairment when tested in the presence of odors (mean without odors = 88.5% (83.4, 93.1); mean with odors = 86.3% (81.0, 91.0); p = 0.401; Wilcoxon signed-rank test). g Illustration of the orthogonality of the decoding vector separating grating orientations (a) with the decoding vector separating odor identities (d). h Dot product of grating orientation and odor identity decoding vectors (black). The scalar product was computed between the odor identity decoding vector across time and the grating orientation decoding vector fixed over the stimulus presentation. The same operation between the grating orientation decoding vector and itself is shown for comparison (blue). Shading indicates 95% CI over 10 random 2-fold train/test splits.

# Supplementary Files

This is a list of supplementary files associated with this preprint. Click to download.

- SupplementaryMaterials.pdf